Applied Surface Science 314 (2014) 872–876

Contents lists available at ScienceDirect

Applied Surface Science

journal homepage: www.elsevier.com/locate/apsusc

High quality ZnO–TiO_2 core–shell nanowires for efficient ultraviolet sensing

Dali Shao [a,*], Hongtao Sun [b], Guoqing Xin [b], Jie Lian [b], Shayla Sawyer [a]

[a] Department of Electrical, Computer and Systems Engineering, Rensselaer Polytechnic Institute, Troy, NY 12180, USA
[b] Department of Mechanical, Aerospace and Nuclear Engineering, Rensselaer Polytechnic Institute, Troy, NY 12180, USA

ARTICLE INFO

Article history:
Received 29 April 2014
Received in revised form 22 June 2014
Accepted 28 June 2014
Available online 10 July 2014

Keywords:
ZnO–TiO_2 core–shell nanowires
UV photodetector
Heterojunction
Photoresponsivity

ABSTRACT

High quality ZnO–TiO_2 core–shell nanowires (NWs) have been fabricated via a facile two-step method: growth of ZnO nanowires by hydrothermal synthesis and then coating of highly uniform TiO_2 shell using atomic layer deposition (ALD) technique. The ultraviolet (UV) emission intensity of the ZnO–TiO_2 core–shell NWs is largely quenched due to an efficient electron–hole separation that reduces the band-to-band recombinations. To the contrary, the absorption of the ZnO–TiO_2 core–shell NWs in both UV and visible region is enhanced, which is attributed to the antireflection properties of the TiO_2 shell. An UV photodetector fabricated from the ZnO–TiO_2 core–shell NWs showed a maximum photoresponsivity as high as 495 A/W at 373 nm under −10 V, which is ~8 times higher than that of the photodetector fabricated from bare ZnO NWs. In addition, the transient response of the ZnO–TiO_2 core–shell NWs is improved by 6 times as compared to that of the bare ZnO NWs. The results presented in this work suggest that ZnO–TiO_2 core–shell NWs may be promising for various optoelectronics applications including: UV photodetectors, optical switches, optical fibers and solar cells.

© 2014 Elsevier B.V. All rights reserved.

1. Introduction

Ultraviolet (UV) photodetectors have been investigated for a variety of commercial and military applications, such as secure space-to-space communications, pollution monitoring, water sterilization, flame sensing and early missile plume detection [1–3]. With a direct wide band gap (3.37 eV), large exciton binding energy (60 meV), high chemical stability and strong resistance to high energy proton irradiation, ZnO has been regarded as one of the most promising candidates for UV photodetector applications [4–7]. Various ZnO nanostructures have been used for fabrication of UV photodetectors with high photoconductive gain and high responsivity [8–10]. However, one of the challenges in widespread use of ZnO for optoelectronic devices is that quick recombination of photogenerated electron–hole pairs occurring in or at the surface of ZnO nanostructures results in a low quantum efficiency [11,12]. To overcome this disadvantage, many research interests have been focused on development of ZnO composite material system [13,14,10]. The incorporation of ZnO into a composite material system in the nanoscale may result a variety of functions different from the original ZnO and possibly induce intriguing properties that inherited from the synergetic effect. For example, the ZnO–TiO_2 material systems have greater physical and chemical properties than that of individual ones, which results from the modification of their electronic states [15,16]. The photogenerated electrons and holes in the ZnO–TiO_2 material systems can be effectively separated "naturally" due to their type-II band alignment, which can greatly enhance the lifetime of the excitonic charge carrier. Recently, ZnO–TiO_2 composite material systems have been reported for a variety of applications including gas sensors, solar cells and photocatalysts [17,18]. While, its application as UV photodetector is rarely investigated. Recently, Panigrahi et al. reported synthesis of ZnO–TiO_2 core–shell nanorodes for UV sensing using spin casting method followed by heating process [19]. However, the TiO_2 shell coated by this route is highly nonuniform, which may significantly reduce the excitonic charge carrier separation and light absorption efficiency in the core–shell system.

Herein, we report the synthesis of ZnO–TiO_2 core–shell NW array for efficient UV sensing using ALD technique. ALD, utilizing sequential self-terminating gas–solid reactions, has emerged as an important thin film deposition technique that achieve uniform coatings on extremely complex shapes with a conformal material layer of high quality, as compared with pulsed laser deposition (PLD), magnetron sputtering, thermal spray, and chemical vapor deposition (CVD) [20–22]. The TiO_2 shells coated via ALD is highly uniform, which not only improved the excitonic charge separation

* Corresponding author.
E-mail addresses: shaod2@rpi.edu, shaodali828@gmail.com (D. Shao).

http://dx.doi.org/10.1016/j.apsusc.2014.06.182
0169-4332/© 2014 Elsevier B.V. All rights reserved.

in the ZnO–TiO_2 core–shell NWs, but also act as an antireflection layer that enhanced the light absorption in the structure.

2. Experimental

2.1. Synthesis of ZnO–TiO_2 core–shell NWs

The synthesis process of the core–shell structure is shown in Scheme 1. First, ZnO NW array were grown on indium tin oxide (ITO) substrate using a hydrothermal growth method [10]. In a typical process, ammonium hydroxide (28 wt%) was added dropwise into 0.1 M zinc chloride solution until the pH is 10–11 and the solution was clear. Subsequently, the transparent solution was transferred to a Teflon-lined autoclave (Parr, USA) and the ITO substrate with ZnO nanoparticles as a seed layer was suspended in the solution at 95 °C for 3 h in a regular laboratory oven. Then the growth solution was cooled down to room temperature naturally. The resulting substrate was thoroughly washed with deionized water and ethanol for several times and dried in air at room temperature. Second, TiO_2 shells were grown directly on ZnO NWs using a SUNALE^{TM} R-200 ALD-reactor (Picosun Ltd) with nitrogen as a carrier and purging gas. The ALD of the TiO_2 shells was performed using alternating $TiCl_4$ and H_2O exposures with a process temperature at 250 °C:

$$TiOH* + TiCl_4 \rightarrow TiOTiCl_3* + HCl \quad (A)$$

$$TiCl* + H_2O \rightarrow ZnOH* + CH_3CH_3 \quad (B)$$

where the asterisks represent the surface species. By repeating these reactions in an ABAB... sequence, TiO_2 can be deposited with atomic layer control. The pulse and purge times in one ALD cycle were 0.2 s $TiCl_4$/10 s purge/0.2 s H_2O/10 s purge. Cycles were repeated 50, 100 and 150 times and the samples were accordingly named as ZnO-TiO_2-50, ZnO-TiO_2-100 and ZnO-TiO_2-150, respectively. After the ALD process, the ZnO–TiO_2 core–shell NWs samples were then annealed in air at 660 °C for 30 min.

2.2. Fabrication of UV photodetectors from the ZnO–TiO_2 core–shell NWs

The UV photodetectors were fabricated by deposition of aluminum (Al) contacts on top of the ZnO–TiO_2 core–shell NWs heterostructures using E-beam evaporation through a shadow mask. The area of the photodetectors is 0.04 cm^2 and the Al contacts had a thickness of 250 nm. Then, the photodetectors were packaged and wire bonded using Epo-Tek H20E conductive epoxy. For comparison purpose, a reference photodetector was fabricated from bare ZnO NWs following the same procedure above.

2.3. Material and device characterizations

A Carl Zeiss Ultra 1540 dual beam scanning electron microscope (SEM) was used to determine the morphology of the bare ZnO NWs and the ZnO–TiO_2 core–shell NWs. Transmission electron microscopy (TEM) and high resolution TEM (HRTEM) studies were carried out in a TEM microscope (JEOL 2011) at an operating voltage of 200 kV. Energy dispersive spectroscopy (EDS) analysis was acquired using an EDS detector inside the TEM microscopy. X-ray diffraction (XRD, PANalytical) patterns of the bare ZnO NWs and the ZnO–TiO_2 core–shell NWs were measured at room temperature using Cu Kα radiation. The photoluminescence (PL) spectra of the samples were measured using a Spex-Fluorolog-Tau-3 spectrofluorimeter with excitation wavelength fixed at 330 nm. The absorption spectra were measured using Shimadzu UV-Vis 2550 spectrophotometer with a deuterium lamp (190–390 nm) and a halogen lamp (280–1100 nm). The typical *I–V* characteristics and transient response of the UV photodetectors were measured using a HP4155B semiconductor parameter analyzer under dark and UV illumination at 335 nm with a power density of around 7.5 μW/cm^2. The photoresponsivity of the devices were measured by Shimadzu UV-Vis 2550 spectrophotometer in connection with a Newport 1928-C optical power meter.

3. Results and discussion

The high resolution SEM images of the ZnO–TiO_2 core–shell NW array are shown in Fig. 1a and b. The ZnO–TiO_2 core–shell NWs are highly vertical aligned and the average diameter of the ZnO–TiO_2 core–shell NWs is 100 nm. The TEM images of a single ZnO–TiO_2 core–shell NW is shown in Fig. 1c and d, which shows that the TiO_2 shell deposited by ALD is highly uniform. The inset of Fig. 1d shows the HRTEM image of the ZnO–TiO_2 core–shell NW, from which the (0 0 2) plane of the wurtzite ZnO structure and (1 0 1) plane of anatase TiO_2 can be clearly observed. Fig. 2a shows the XRD pattern ZnO–TiO_2 core–shell NW array. All the peaks are identified and assigned according to the Joint Committee of Powder Diffraction Standards (JCPDS) data. The diffraction peaks (purple) at $2\theta = 25.3°$ (1 0 1) and 37.8° (1 0 4) can be indexed to the anatase TiO_2 (JCPDS #21-1272) while the rest peaks (red) are well indexed to the wurtzite ZnO (JCPDS #36-1451). Energy dispersive spectroscopy (EDS) analysis in Fig. 2b confirmed that only zinc, oxygen and titanium existed in the core–shell NWs.

The room-temperature PL spectra of the bare ZnO NWs and the ZnO–TiO_2 core–shell NWs are shown in Fig. 3a. When excited at 330 nm, the PL spectra of the samples show a UV emission band centered at 380 nm and a broad visible emission band with peak wavelength at 530 nm. The UV emission band is attributed to the near band (NB) emission of the ZnO crystal while the broad visible emission band is defect level emission that originates from oxygen vacancies in the structures [14]. The PL intensity of the synthesized ZnO–TiO_2 NWs keep decreasing as the thickness of the coated TiO_2 shell increases. The main reason for this phenomenon is attributed to the charge-separation effect of the type-II band alignment of ZnO and TiO_2. As illustrated in the inset of Fig. 3a, due to the staggered band offset, the photogenerated electrons and holes will be separated and connected mainly in the TiO_2 shell and ZnO core respectively to form an excitonic charge separation state. Such an efficient charge separation decreases the recombination rate of electrons and holes and weakens the PL intensity of the ZnO–TiO_2 core–shell NWs consequently [18,19]. In addition, multiple reflections created by the TiO_2 shell may lead to a weaker PL intensity by increasing light absorption efficiency, as shown in Fig. 3b. The refraction index of anatase TiO_2 (~2.55) is higher than that of the wurtzite ZnO (~1.99). Therefore, the TiO_2 shell also acts as antireflection layer and the light can be effectively confined in the ZnO–TiO_2 core–shell NWs and scattered until most of the light is absorbed. Similar phenomena have also been observed from other core–shell structures such as such as ZnO–ZnSe and Zn_3P_2–ZnO [23,24].

The schematic illustration of the photodetector fabricated from the ZnO–TiO_2 core–shell NWs is shown in Fig. 4a. The typical *I–V* characteristics of the UV photodetectors fabricated from the bare ZnO NWs and the ZnO–TiO_2 NWs are shown in Fig. 4b. It is obvious that the dark current of all the photodetectors present rectifying effect. Considering the *n*-type nature of undoped ZnO and the electron affinity of ITO, Schottky contact forms in the interface between ZnO and ITO [25]. As shown in Fig. 4b, the photodetector fabricated from ZnO–TiO_2 NWs show both higher photocurrent and dark current than that of the reference photodetector fabricated from bare ZnO NWs. The maximum photocurrent to dark current ratio of the photodetectors is observed from ZnO-TiO_2-100 (2.3×10^4

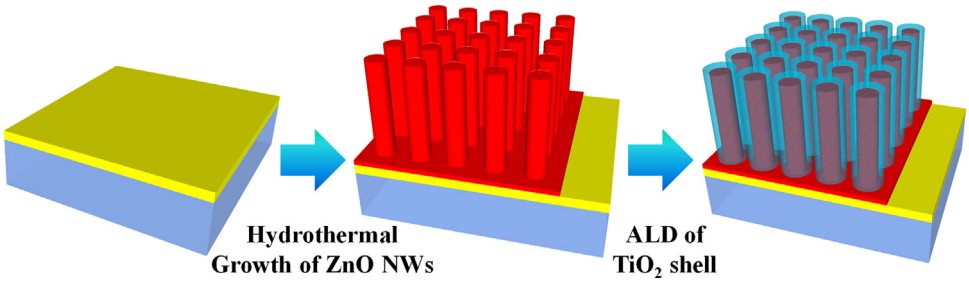

Scheme 1.

at −10 V), which is 8.5 times higher than that of the reference photodetector. The enhancement in photocurrent of the ZnO–TiO_2 core–shell NWs, as discussed earlier, is attributed to both efficient excitonic charge separation and the antireflection property of the TiO_2 shell. The photocurrent of ZnO-TiO_2-150 is lower than that of ZnO-TiO_2-100. As the number of coatings increase, most of the electrons produced in the shell are trapped by the adsorbed oxygen molecules on the surface of TiO_2 and thus could not be transferred to ZnO [19]. The slightly higher dark current of the ZnO–TiO_2 core–shell NWs is probably due to surface modification of ZnO NWs after TiO_2 shell coating, which reduces the trapping of charge carriers by surface adsorbed oxygen molecules [26]. This effect can greatly benefit transient response of ZnO based photodetectors, as the persistent photoconductivity (PPC) phenomenon can be suppressed [27]. As demonstrated in Fig. 5, the rise time (from 10% to 90%) and fall time (from 90% to 10%) of the photodetector fabricated from ZnO–TiO_2 core–shell NWs are at least 3 times faster than the reference photodetector fabricated from the bare ZnO NWs. It is worth to mention that the transient response of the device may be further improved by coating a thin layer of graphene outside the TiO_2 shell through a facile three-step method reported in our previous work [14]. Further optimization of the device is underway.

The photoresponsivity spectra of the photodetectors, defined as photocurrent per unit of incident optical power, are shown in Fig. 6. A maximum photoresponsivity of 495 A/W at 373 nm was achieved for the UV photodetector fabricated form the ZnO-TiO_2-100 when under −10 V bias, this is 8 times higher than that of the reference photodetector and is more than three orders of magnitude higher than those of commercial GaN or SiC photodetectors (<0.2 A/W) [9]. The high UV responsivity of the ZnO–TiO_2 core–shell NWs demonstrated its promising applications for UV photodetectors and optical switches. The inset of Fig. 6 shows the external quantum efficiency (EQE) of the photodetector calculated using the equation $EQE = R \times hv/q$, where hv is the energy of the incident photon in electronvolts, q is the electron charge and R is the photoresponsivity of the UV photodetector [28]. The specific detectivity

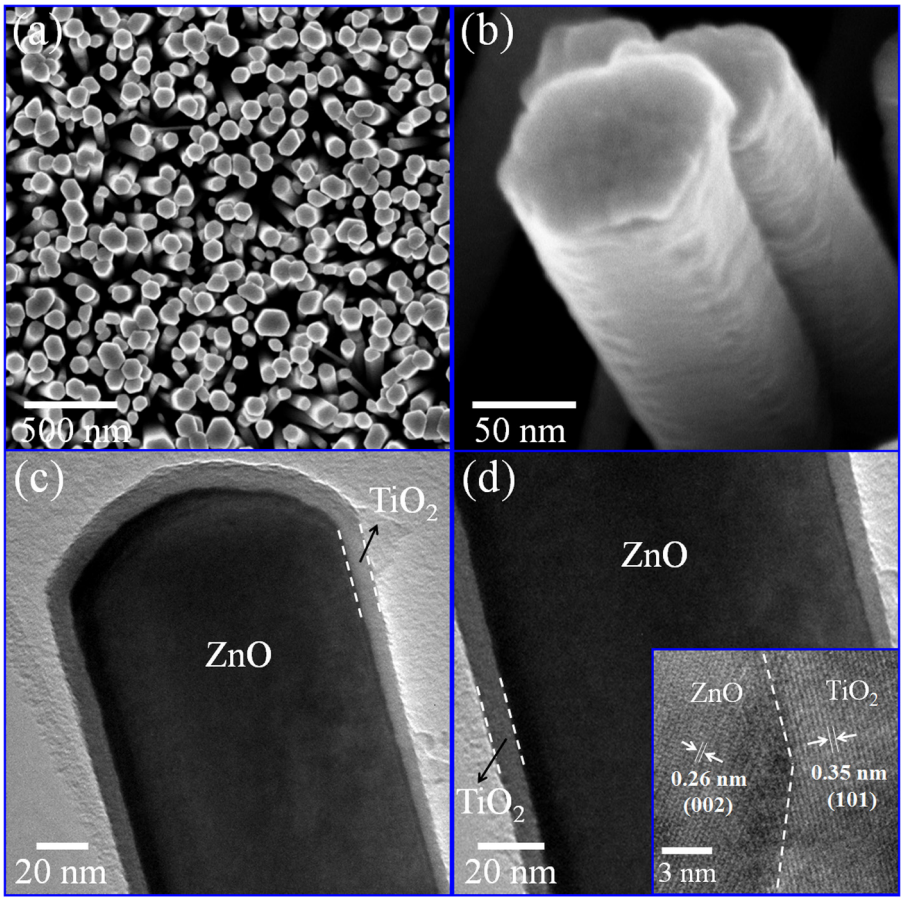

Fig. 1. (a and b) SEM images of the highly vertical aligned ZnO–TiO_2 core–shell NWs. (c and d) TEM images of a single ZnO–TiO_2 core–shell NW. Inset: HRTEM image of the ZnO–TiO_2 core–shell NWs.

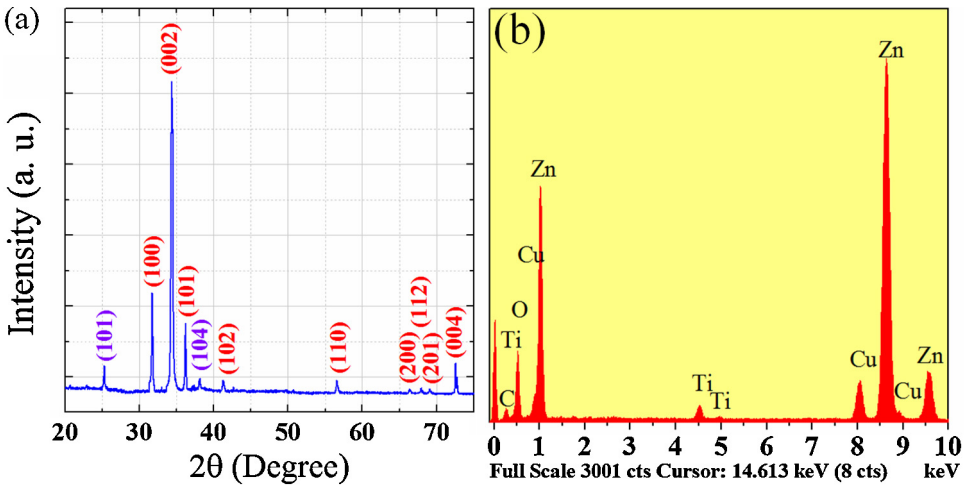

Fig. 2. (a) XRD pattern and (b) EDS analysis of the ZnO–TiO_2 core–shell NWs.

(D^*) of a photodetector is another important figure of merit and can be expressed by the following formula [29]:

$$D^* = \frac{R\sqrt{A \times \Delta f}}{i_n}$$

where the i_n is the noise current in the unit of A/$Hz^{1/2}$, Δf is operating bandwidth in hertz and A is the area of the device in cm^2. If the dark current is the major contribution for the noise ($i_n = \sqrt{2qi_{dc}\Delta f}$), the D^* can be expressed as [29,30]:

$$D^* = R\left(\frac{A}{2qi_{dc}}\right)^{1/2}$$

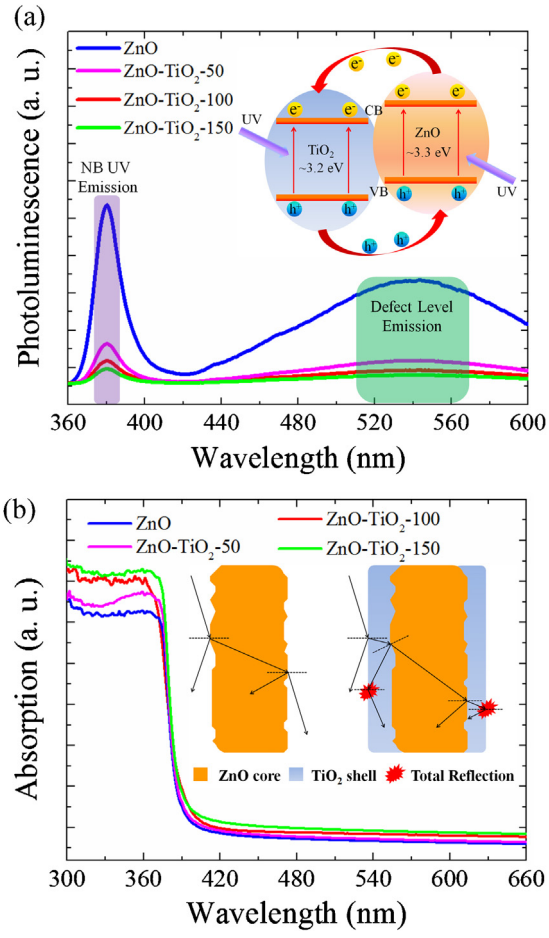

Fig. 3. (a) PL spectra and (b) absorption spectra of the bare ZnO NWs and the ZnO–TiO_2 core–shell NWs. Inset: Schematic illustration of the charge separation in the ZnO–TiO_2 core–shell NWs. Inset: the transmission path of light as it enters a ZnO nanowire (left) and a ZnO–TiO_2 core–shell nanowire (right). The red stars mark the place where total reflection occurs. (For interpretation of the references to color in this figure legend, the reader is referred to the web version of the article.)

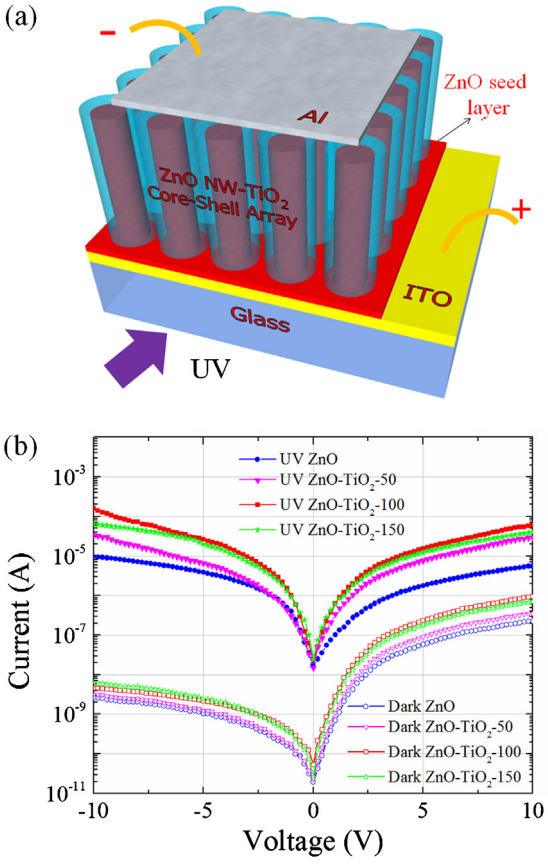

Fig. 4. (a) Schematic illustration of the photodetector fabricated from ZnO–TiO_2 core–shell NWs. (b) Typical I–V characteristics of the photodetectors fabricated from the bare ZnO NWs and from the ZnO–TiO_2 core–shell NWs.

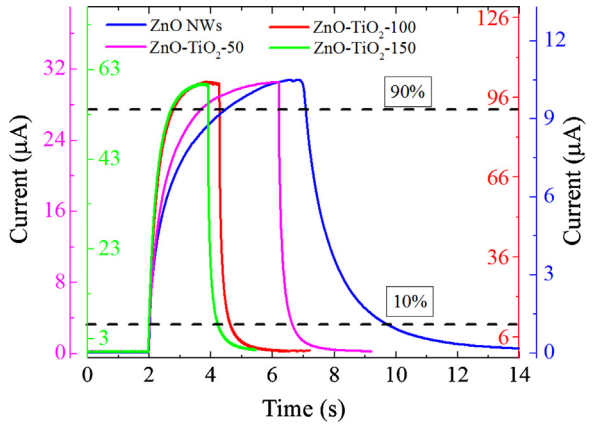

Fig. 5. Transient response of the photodetectors fabricated from the bare ZnO NWs and from the ZnO–TiO_2 core–shell NWs.

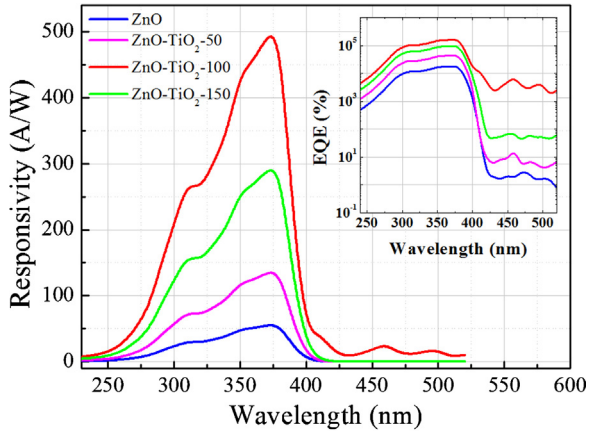

Fig. 6. Photoresponsivity spectra of the photodetectors fabricated from the bare ZnO NWs and from the ZnO–TiO_2 core–shell NWs.

where q is the electron charge and i_{dc} is the dark current of the device. A detectivity of 9.78×10^{14} Jones can be obtained at 373 nm for the photodetector when biased −10 V.

4. Conclusions

We have demonstrated the fabrication of high quality ZnO–TiO_2 core–shell NWs using hydrothermal growth method followed by atomic layer deposition technique. The uniform coating of TiO_2 shell on ZnO NWs can benefit efficient excitonic charge separation and minimize the recombination in the core–shell heterostructure. In addition, the TiO_2 shell also acts as antireflection layer that effectively enhance the light absorption efficiency. A UV photodetector fabricated from the ZnO–TiO_2 core–shell NWs demonstrated greatly improved photocurrent to dark ratio, transient response and photoresponsivity as compared to a reference photodetector fabricated from bare ZnO NWs. The results presented in this work are important not only for stimulating further efforts to utilize ZnO–TiO_2 core–shell structure for UV photodetector applications but also to investigate similar structures for various optoelectronic applications such as optical switch, solar cells and optical fibers.

Acknowledgements

The authors gratefully acknowledge support from National Security Technologies through NSF Industry/University Cooperative Research Center Connection One. The authors also acknowledge the National Science Foundation Smart Lighting Engineering Research Center (EEC-0812056) and a NSF career award DMR 1151028.

References

[1] E. Monroy, F. Calle, J.L. Pau, E. Munoz, F. Omnes, B. Beaumont, P. Gibart, J. Cryst. Growth 230 (2001) 537–543.
[2] G. De Cesare, D. Caputo, A. Nascetti, C. Guiducci, B. Ricco, Appl. Phys. Lett. 88 (2006) 083904.
[3] J.P. Liu, S.S. Wang, Z.Q. Bian, M.N. Shan, C.H. Huang, Chem. Phys. Lett. 470 (2009) 103–106.
[4] C.-Y. Chang, F.-C. Tsao, C.-J. Pan, G.-C. Chi, H.-T. Wang, J.-J. Chen, F. Ren, D.P. Norton, S.J. Pearton, K.-H. Chen, L.-C. Chen, Appl. Phys. Lett. 88 (2006) 173503.
[5] D. Shao, H. Sun, M. Yu, J. lian, S. Sawyer, Nano Lett. 12 (2012) 5840–5844.
[6] D.C. Look, C. Coskun, B. Claflin, G.C. Farlow, Physica B 340 (2003) 32–38.
[7] D. Shao, M. Yu, J. Lian, S. Sawyer, IEEE Electron Dev. Lett. 34 (2013) 1169–1171.
[8] C. Soci, A. Zhang, B. Xiang, S.A. Dayeh, D.P.R. Aplin, J. Park, X.Y. Bao, Y.H. Lo, D. Wang, Nano Lett. 7 (2007) 1003–1009.
[9] Y.-Q. Bie, Z.-M. Liao, H.-Z. Zhang, G.-R. Li, Y. Ye, Y.-B. Zhou, J. Xu, Z.-X. Qin, L. Dai, D.-P. Yu, Adv. Mater. 23 (2011) 649–653.
[10] D. Shao, M. Yu, J. Lian, S. Sawyer, Appl. Phys. Lett. 102 (2013) 021107.
[11] L. Lin, Y. Yang, L. Men, X. Wang, D. He, Y. Chai, B. Zhao, S. Ghoshroy, Q. Tang, Nanoscale 5 (2013) 558–593.
[12] R. Liu, H. Ye, X. Xiong, H. Liu, Mater. Chem. Phys. 121 (2010) 432–439.
[13] K.S. Leschkies, R. Divakar, J. Basu, E. Enache-Pommer, J.E. Boercker, C.B. Carter, U.R. Kortshagen, D.J. Norris, E.S. Aydil, Nano Lett. 7 (2007) 1793–1798.
[14] D. Shao, M. Yu, H. Sun, T. Hu, J. lian, S. Sawyer, Nanoscale 5 (2013) 3664–3667.
[15] Y.Z. Li, W. Xie, X.L. Hu, G.F. Shen, X. Zbou, Y. Xiang, X.J. Zhao, P.F. Fang, Langmuir 26 (2010) 591–597.
[16] M. Agrawal, S. Gupta, A. Pich, N.E. Zafeiropoulos, M. Stamm, Chem. Mater. 21 (2009) 5343–5348.
[17] J.Y. Park, S.-W. Choi, J.-W. Lee, C. Lee, S.S. Kim, J. Am. Ceram. Soc. 92 (2009) 2551–2554.
[18] L.E. Greene, M. Law, B.D. Yuhas, P. Yang, J. Phys. Chem. C 111 (2007) 18451–18456.
[19] S. Panigrahi, D. Basak, Nanoscale 3 (2011) 2336–2341.
[20] S.M. George, Chem. Rev. 110 (2010) 111–131.
[21] J.W. Elam, J.W. Elam, D. Routkevitch, P.P. Mardilovich, S.M. George, Chem. Mater. 15 (2003) 3507–3517.
[22] R.G. Gordon, D. Hausmann, E. Kim, J. Shepard, Chem. Vap. Depos. 9 (2003) 73–78.
[23] K. Wang, J.J. Chen, W.L. Zhou, Y. Zhang, Y.F. Yan, J. Pern, A. Mascarenhas, Adv. Mater. 20 (2008) 3248–3253.
[24] P.C. Wu, T. Sun, Y. Dai, Y.H. Sun, Y. Ye, L. Dai, Cryst. Growth Des. 11 (2011) 1417–1421.
[25] J.-G. Yoon, S.W. Cho, E. Lee, J.-S. Chung, Appl. Phys. Lett. 95 (2009) 222102.
[26] F.K. Shan, G.X. Liu, W.J. Lee, G.H. Lee, I.S. Kim, B.C. Shin, Appl. Phys. Lett. 86 (2005) 221910.
[27] J.D. Prades, F. Hernandez-Ramirez, R. Jimenez-Diaz, M. Manzanares, T. Andreu, A. Cirera, A. Romano-Rodriguez, J.R. Morante, Nanotechnology 19 (2008) 465501.
[28] D. Shao, X. Sun, M. Xie, M. Yu, S.M. George, J. Lian, S. Sawyer, Mater. Lett. 112 (2013) 165–168.
[29] X. Gong, M. Tong, Y. Xia, W. Cai, J.S. Moon, Y. Cao, G. Yu, C.-L. Shieh, B. Nilsson, A.J. Heeger, Science 325 (2009) 1665–1667.
[30] T. Yang, K. Sun, X. Liu, W. Wei, T. Yu, X. Gong, D. Wang, Y. Cao, J. Phys. Chem. C 116 (2012) 13650–13653.